Electronic Supplementary Material (ESI) for Energy & Environmental Science.

Supplementary Information

Enhanced sub-bandgap efficiency of a solid-state organic intermediate band solar cell using triplet-triplet annihilation

YunHui L. Lin, Marius Koch, Alyssa N. Brigeman, David M. E. Freeman, Lianfeng Zhao, Hugo Bronstein, Noel C. Giebink, Gregory D. Scholes, and Barry P. Rand*

*brand@princeton.edu

TABLE OF CONTENTS

Section 1. Steady-State Absorption Spectra

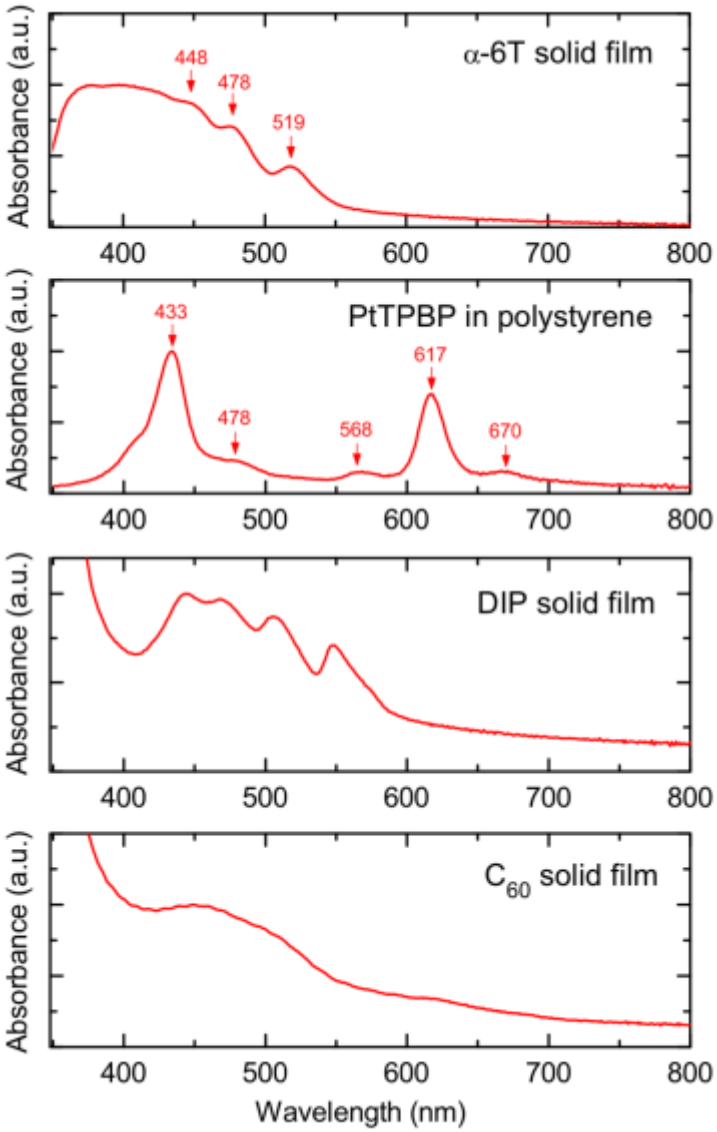

Fig. S1: Steady-state absorption of various materials in film form.

Section 2. Transient Absorption and Delayed Fluorescence Additional Information

For the femtosecond transient absorption experiments the 800 nm output of a 1 kHz, 45 fs LIBRA Ti:Sapphire amplified system (Coherent Inc.) was split into two beams. The first part was sent into an OPerA Solo optical parametric amplifier (Coherent Inc.) to give pump pulses of ~70 fs centered at 520 and 620 nm. A small fraction of the second part was sent into a Helios transient absorption spectrometer (Ultrafast Systems) and focused into a 3 mm Sapphire crystal for white light continuum generation (spectrum shown in Supplementary Fig. S5). Narrowband pump and broadband probe pulses were focused and overlapped on the sample with beam polarizations at magic angle condition. The beam diameter is defined as the diameter where the pulse energy drops by $1/e^2 \sim 13.5\%$. The transmitted probe light was focused into an optical fiber connected to a detector. Difference absorption spectra (ΔA) were calculated in real time by chopping every other pump pulse, thereby alternating between measuring the probe/pump-on and probe/pump-off spectra. Spectra were averaged for 0.2 to 0.4 seconds before changing the delay time between pump and probe using an automatized translation stage. Each scan consists of spectra collected at pump-probe delays between -5 to 7300 ps.

Multiple scans were averaged to increase the signal to noise ratio and corrected for background and chirp using the analysis software SURFACE XPLORER (Ultrafast Systems). No sample degradation was observed throughout the experiment, verified by comparing the scans prior to averaging.

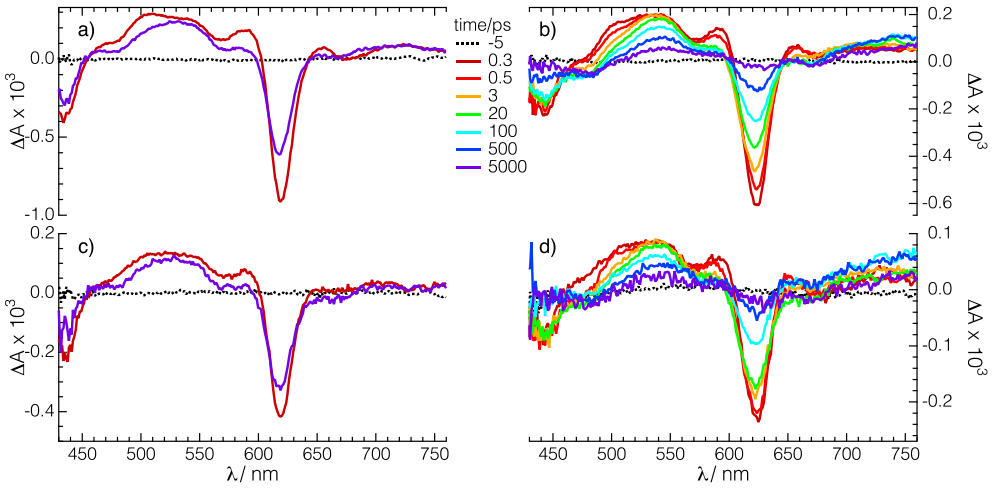

Fig. S2: Transient absorption spectra recorded after 620 nm excitation of PtTPBP in a polystyrene matrix (left, a&c) and 5 wt% PtTPBP:α-6T (right, b&d). The excitation energy per pulse was 25 nJ (top, a&b) and 12.5 nJ (bottom, c&d), corresponding to a fluence of roughly 0.033 & 0.016 mJ/cm^2, respectively.

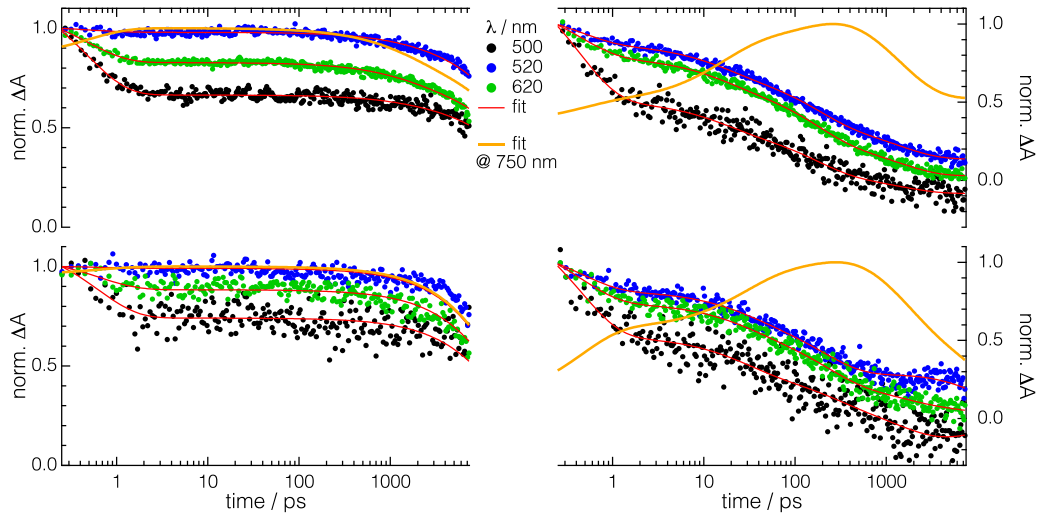

Fig. S3: Time evolution of transient absorption spectra of Fig. S2 recorded upon excitation at 620 nm. **Left**: PtTPBP in polystyrene matrix. **Right**: α-6T:PtTPBP(5 wt%). Thin red lines represent fits of three (a&c) and five (b&d) exponentials to the experimental data, derived from a global analysis of the entire data set. The negative bleach amplitudes at 620 nm (green) are inverted for better visualization. Due to the low signal-to-noise ratio at 750 nm, only the fit to the experimental data is shown in orange for better visualization. The excitation energy per pulse was 25 nJ (top, a&b) and 12.5 nJ (bottom, c&d).

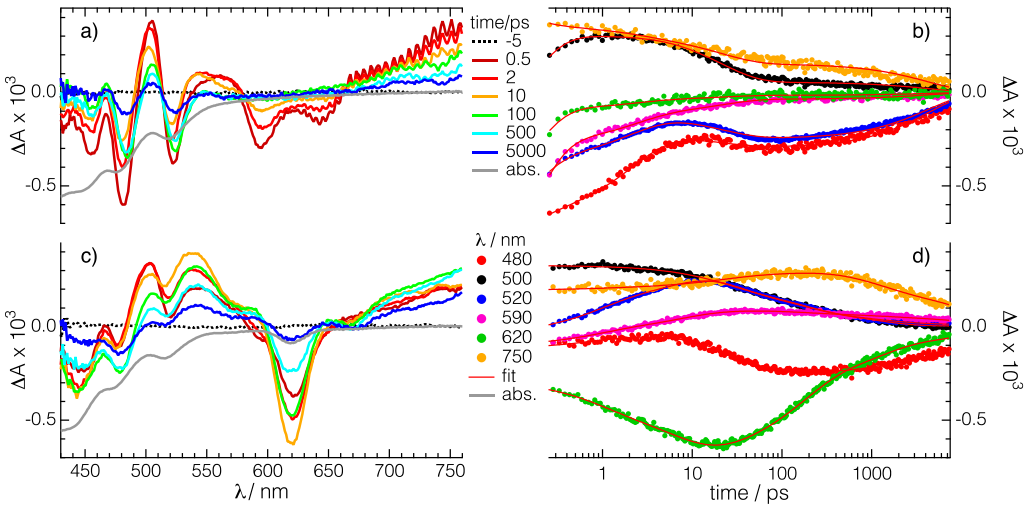

Fig. S4: Transient absorption spectra (left) and their temporal evolution (right) upon excitation at 520 nm, **a&b**: α-6T, **c&d**: α-6T:PtTPBP(5 wt%). The excitation energy per pulse was 150 nJ, corresponding to a fluence of roughly 0.019 mJ/cm². Direct excitation of PtTPBP contributes by a maximum of 25% (data not shown) at time zero, while the increase at later times is exclusively due to secondary sensitization of PtTPBP. Thin red lines stand for fits of four (b) and six (d) exponentials to the experimental data, coming from a global analysis of the entire data set. The steady-state absorption of the corresponding sample is shown as the inverse in grey.

Assignment of the 700 nm positive transient to α-6T triplet excited state absorption

In Fig. S4a, we see that at timescales beyond 500 ps (cyan and blue), no singlet excited state population of α-6T is left (i.e. no stimulated emission, negative features between 580-650 nm). Nevertheless, the ground state, S_0, has not completely refilled (i.e. the negative bleaches remain at 480, 520 nm). It is only reasonable to assume that some α-6T singlets have undergone intersystem crossing to the triplet state, as is known to occur due to the sulfur atom in α-6T. The rising signal beyond 700 nm corresponds then to the excited state absorption of α-6T triplets. If we refer now to Fig. S4c and Fig. 2e (main text), we see also that no stimulated emission from a-6T is detectable (thus, no singlets), but the ground state of α-6T is depopulated. Therefore, ruling out the presence of α-6T singlets on the basis of these results, but having identified an α-6T feature (after PtTPBP excitation), as explained in the main text, the 700 nm positive transient can only reasonably to attributed to the excited state absorption of α -6T triplets.

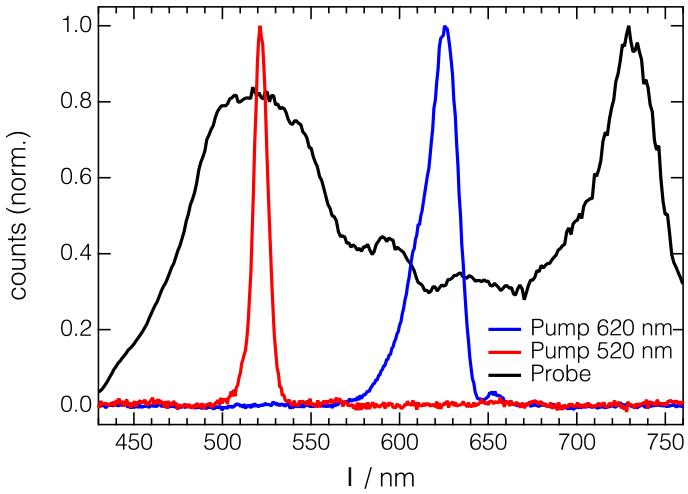

Fig. S5: Spectra of the pump beam at 520 nm (red) and 620 nm (blue) and spectrum of the white light continuum probe beam.

Table S1: Results from global analysis of the data shown in Main Text Fig. 2 and Supplementary Fig. S2 & S3 excited at different excitation energies at 620 nm.

	Time constants (ps)	
	PtTPBP(5%):PS film	**PtTPBP(5%):α6T film**
100 nJ	0.5, 330, >10000	0.4, 8, 85, 760, >10000
25 nJ	0.5, 1500, >10000	0.4, 15, 160, 1400, >10000
12.5 nJ	0.6, >10000	0.5, 25, 210, 1500, >10000

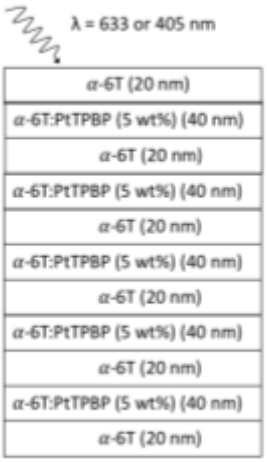

Fig. S6: Full film stack used in power dependent delayed fluorescence spectroscopy study

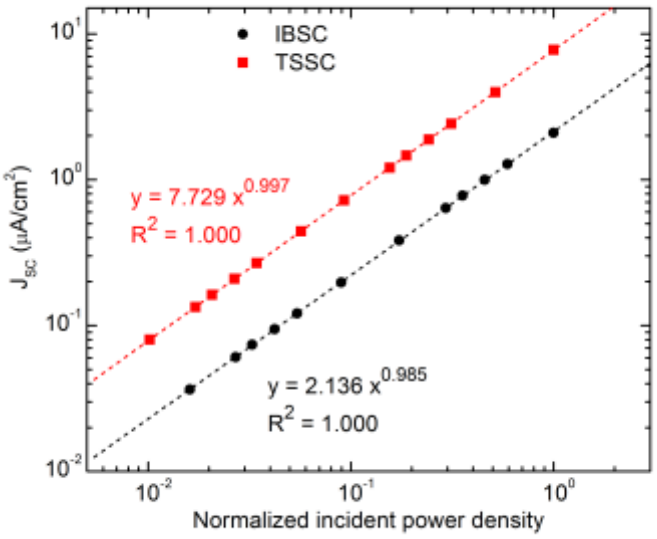

Fig. S7: Photocurrent output from the intermediate band solar cell (IBSC) and triplet sensitized solar cell (TSSC) under selective excitation of the PtTPBP, as a function of incident power density.

One of the most common methods invoked to mechanistically support the sensitized TTA-UC process is the demonstration of a quadratic-to-linear relationship between the incident power of the excitation beam and the upconverted fluorescence intensity. This technique has been used widely in both solution [1-4] and film [5-7] upconversion systems. More recently, similar power-dependent studies have also been used to monitor photocurrent generation in solar cells with TTA-UC antenna layers [8] and IBSCs [9-12], under the assumption that

photocurrent enhancements are proportional to the upconverted singlet population in the same manner as the fluorescence intensity.

A mathematical treatment of the kinetics of TTA-UC systems is given in [3], with the result that in the weak TTA efficiency limit, the upconverted fluorescence intensity scales quadratically with the absorbed optical power, while in the strong TTA efficiency limit, the relationship is linear. These two regimes are defined as follows: in the weak TTA limit, the bimolecular rate of TTA is smaller than that of other triplet decay pathways (e.g. phosphorescence, exciton-polaron annihilation, quenching by molecular oxygen) while in the strong TTA limit, upconversion via TTA is dominant. The TTA efficiency is enhanced at higher excitation powers due to the larger population of triplets, such that a transition from the quadratic to linear regimes is often observed experimentally.

We performed power-dependent photocurrent measurements on the IBSC and TSSC devices with an α-6T spacer layer of 5 nm, with results shown in Fig. S6a. The devices were excited with varying intensities of 615 nm light from a Quartz Tungsten Halogen lamp passed through a monochromator. The measured IBSC short circuit photocurrent exhibited linear behavior throughout the range of excitation intensities. The fact that quadratic behavior is observed in the purely optical experiment (Fig. 3c of the main text) whereas linear behavior is observed in the photocurrent experiment involving the full device structure, suggests that there are losses to photocurrent with overall sublinear intensity dependence. These losses are partly attributed to exciton polaron annihilation (EPA), as illustrated in the 615 nm EQE response of these devices under white light bias and voltage bias (Fig. 5b of the main text). EPA is not present in dye-sensitized solar cells, since the generated charge is extracted through the oxide and therefore physically separated from the site of upconversion. Previous work on organic IBSCs have utilized dye-sensitized solar cells, and therefore were not subject to EPA losses, which may explain why it was possible to observe superlinear power dependent photocurrent in these systems.

The rate model that is invoked to explain the quadratic-to-linear power dependent behavior seen in other works is a relatively simple one involving just the population of triplets in the TTA-UC host. However, this rate model is likely insufficient to describe the power dependent behavior of the solid-state IBSC, where EPA is known to dominate sub-bandgap photocurrent response at high excitation powers. Development of a new rate model that incorporates EPA and charge transfer (CT) of singlets is underway.

Section 3. Verification of α-6T coverage on PtTPBP

The spacer concept introduced in our solid-state molecular IBSC is designed to separate the site of triplet sensitization from the site of TTA-UC. To confirm that α-6T provides complete coverage over the layer doped with PtTPBP, we performed depth-resolved elemental analysis using x-ray photoelectron spectroscopy (XPS). XPS measurements were performed using a Thermo Scientific K-Alpha X-ray Photoelectron Spectrometer (XPS) System with depth profiling and charge compensation capabilities enabled by an argon ion source and a flood gun. A vacuum transfer module was used for sample transfer without ambient exposure to avoid surface contamination and oxidation. The depth of each etch cycle was calibrated against an α-6T film of known thickness and determined to be 2.8 nm/etch cycle. In a film consisting of 70 nm of neat α-6T deposited on an underlayer of α-6T:PtTPBP(5 wt%), the signal from the Pt 4f transition appears at the 24th etch cycle, or 67 nm below the surface. This confirms that in devices utilizing an α-6T spacer layer, complete coverage of the PtTPBP-doped underlayer is achieved within only a couple of nm.

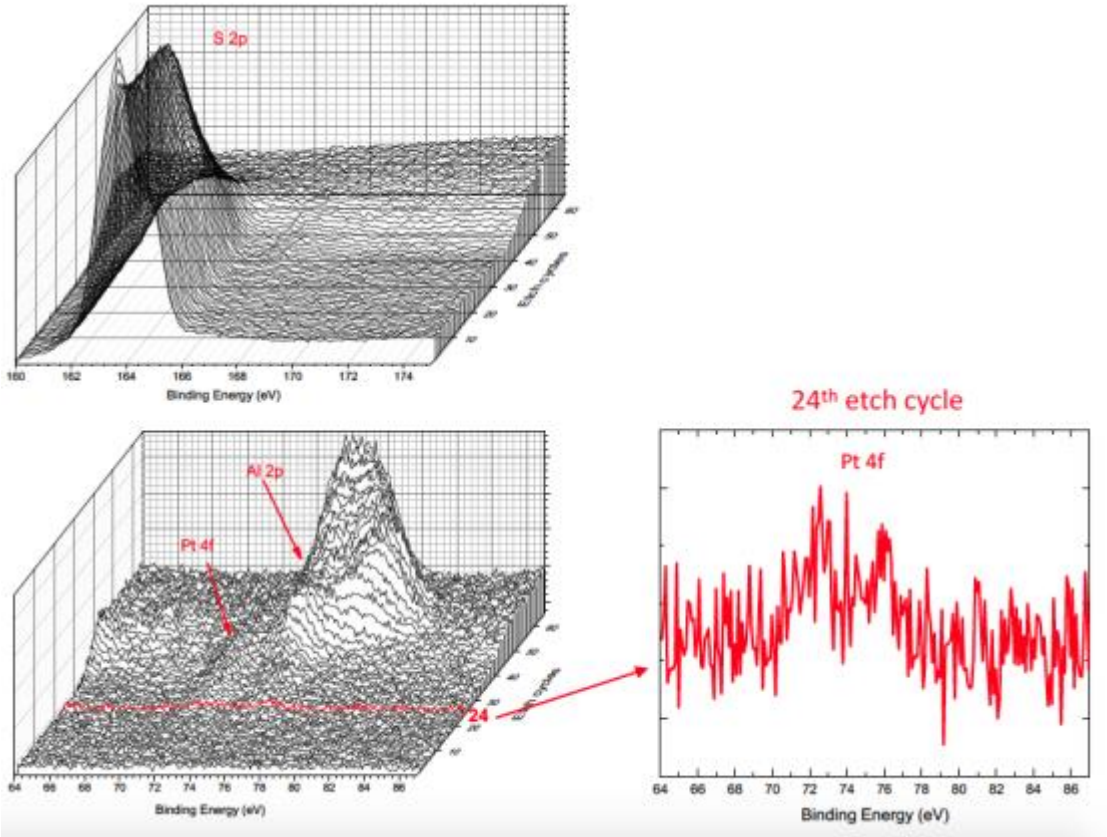

Fig. S8: Layer-by-layer elemental analysis of a film of neat α-6T deposited on a layer of PtTPBP-doped α-6T. The sulfur 2p signal (attributed to α-6T) exists throughout the entire film while the platinum 4f signal (attributed to PtTPBP) only appears after the 24th etch cycle. Note that the growing signal in the platinum panel is in fact an aluminum 2p transition, which appears due to the Al_2O_3 content of the underlying substrate (alkaline earth boroaluminosilicate glass).

Section 4. Device Performance Characteristics

Device current-voltage characteristics were measured using a Keithley 2602B sourcemeter. Simulated AM1.5 illumination was provided by a calibrated ABET Technologies 11000 solar simulator.

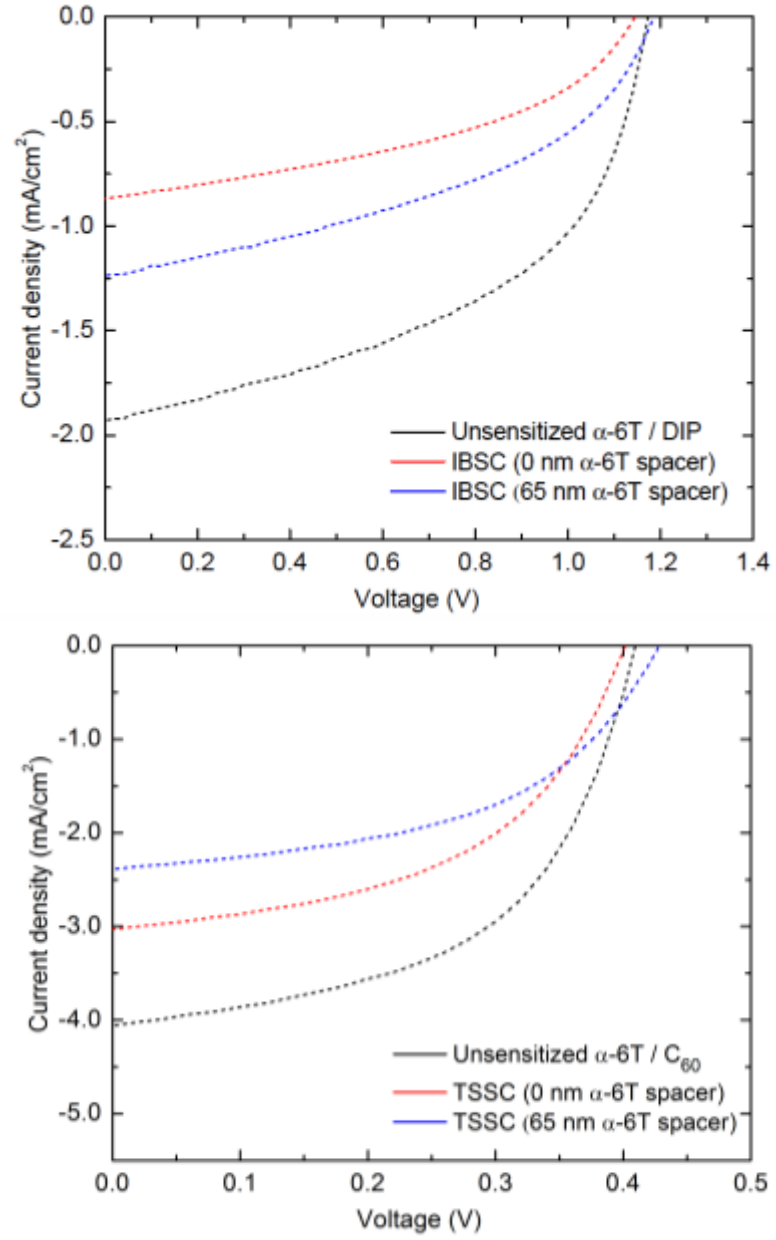

Fig. S9: Representative current density-voltage curves of α-6T/DIP devices (top) and α-6T/C_{60} devices (bottom) under 1 sun illumination.

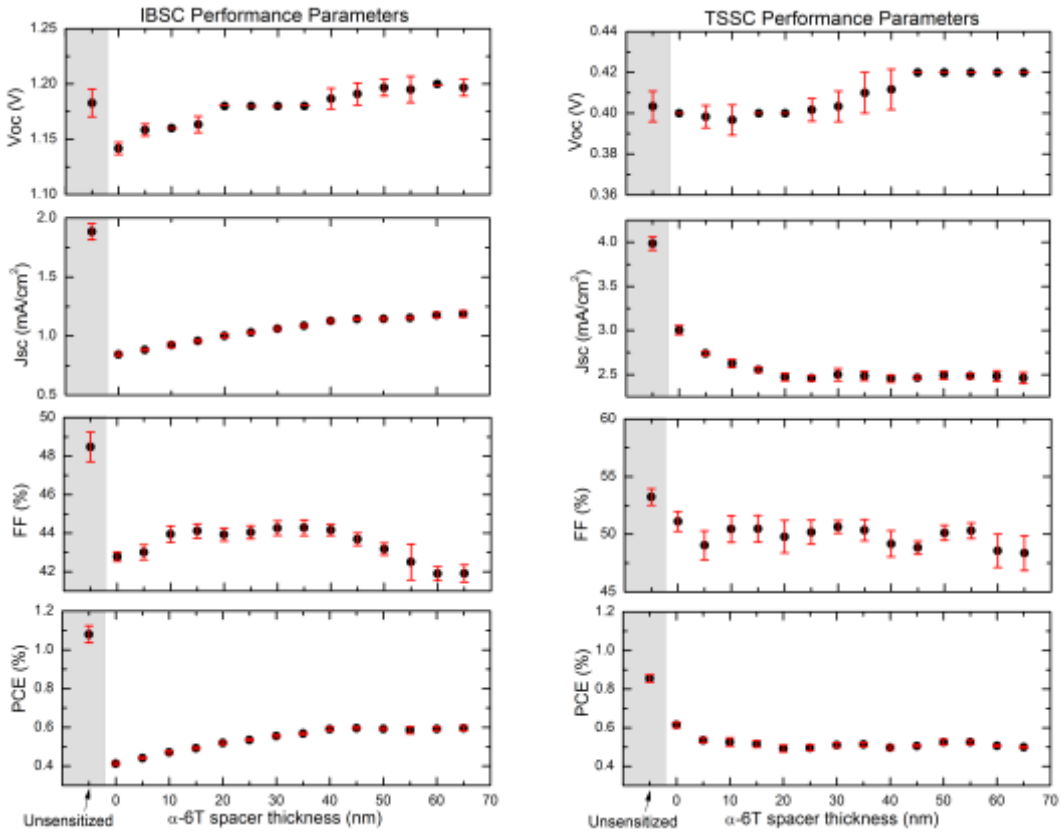

Fig. S10: Device performance parameters. The first data point in each plot corresponds to unsensitized devices (i.e. no PtTPBP present). Subsequent devices are, on left, intermediate band solar cells (IBSC) and on right, triplet sensitized solar cells (TSSC) with various α-6T spacer layer thicknesses. Performance parameters shown are open circuit voltage (V_{OC}), short circuit current density (J_{SC}), fill factor (FF), and power conversion efficiency (PCE). Each data point represents averages (dots) and standard deviations (red error bars) on 11-12 simultaneously fabricated devices.

There are two noteworthy behaviors to be seen here. First, the open circuit voltages (V_{OC}) of both the α-6T/DIP and α-6T/C60 devices show essentially no change upon doping the α-6T with PtTPBP. Second, the short-circuit currents (J_{SC}) of the IBSC and TSSC devices show opposite trends with spacer thickness: the IBSC devices show increased photocurrent with spacer thickness while the TSSC devices show reduced photocurrent with spacer thickness. Even though these J_{SC} trends are impacted by many different factors (e.g. the amount of light absorbed, differences in exciton diffusion efficiency), the trends are consistent with our expectation that the amount of TTA-UC scales with the thickness of the α-6T spacer.

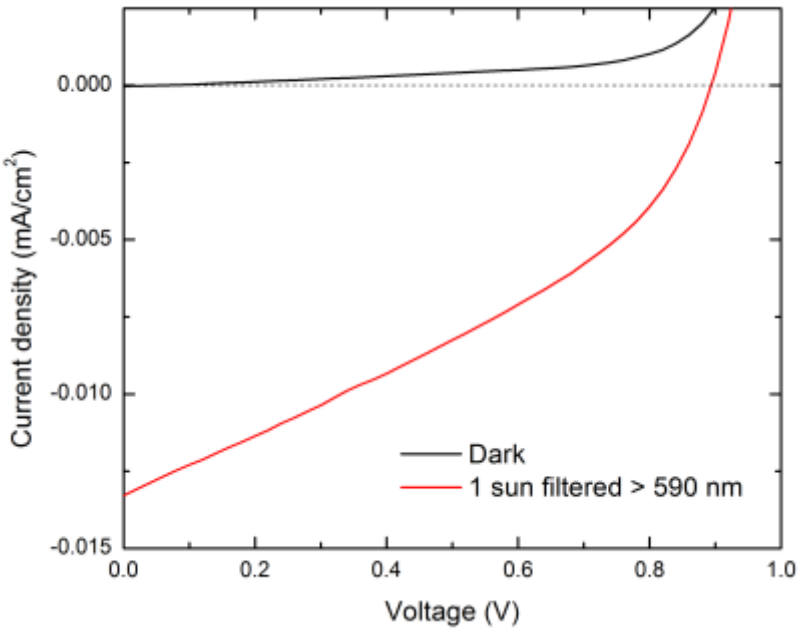

Fig. S11: Current density-voltage measurements of the intermediate band solar cell (IBSC) with 5 nm α-6T spacer layer. In the red curve, the 1 sun AM1.5G excitation source is filtered with a 590 nm long pass filter, so as to restrict the excitation to the PtTPBP sensitizer. The relevant device parameters are shown in the chart below.

	1 Sun AM1.5G	**1 Sun with > 590 nm filter**
J_{SC} (mA/cm²)	0.82	0.0133
V_{OC} (V)	1.11	0.882
FF (%)	42	35
PCE (%)	0.385	N/A

Figure S11 shows the current density – voltage response of the IBSC with 5 nm a-6T spacer under 1 Sun AM1.5 illumination passed through a 590 nm long pass filter. The J_{sc} given above for the filtered excitation represents a slight underestimate, given that the transmission of the filter is not 100%. The V_{oc} is reduced, as expected due to the lower illumination and corresponding photocurrent, but still maintains a relatively high value compared to the unfiltered 1 Sun case. The J_{sc} produced under filtered illumination represents approximately 1.6% of that produced under the full 1 Sun spectrum. The value obtained from integrating the EQE spectrum in the range 590 – 750 nm is similar, although small differences arise due to the imperfect transmission curve and cutoff wavelength of the 590 nm long pass filter.

References

1. T. N. Singh-Rachford and F. N. Castellano, *J. Phys. Chem. Lett*., 2010, **1**, 195-200.
2. Y. Y. Cheng, T. Khoury, R. G. C. R. Clady, M. J. Y. Tayebjee, N. J. Ekins-Daukes, M. J. Crossley and T. W. Schmidt, *Phys. Chem. Chem. Phys.*, 2010, **12**, 66-71.
3. A. Haefele, J. Blumhoff, R. S. Khnayzer and F. N. Castellano*, J. Phys. Chem. Lett*., 2012, **3**, 299-303.
4. Z. Jiang, M. Xu, F. Li and Y. Yu, *J. Am. Chem Soc.,* 2013, **135**, 16446-16453.
5. R. R. Islangulov, J. Lott, C. Weder and F. N. Castellano, *J. Am. Chem. Soc.*, 2007, **129**, 12652-12653.
6. M. Wu, D. N. Congreve, M. W. B. Wilson, J. Jean, N. Geva, M. Welborn, T. Van Voorhis, V. Bulović, M. G. Bawendi and M. A. Baldo, *Nat. Photon*., 2016, **10**, 31-34.
7. P. Mahato, A. Monguzzi, N. Yanai, T. Yamada, and N. Kimizuka, *Nat. Mater.*, 2015, **14**, 924-930.
8. A. Nattestad, Y. Y. Cheng, R. W. MacQueen, T. F. Schulze, F. W. Thompson, A. J. Mozer, B. Fückel, T. Khoury, M. J. Crossley, K. Lips, G. G. Wallace and T. W. Schmidt, *J. Phys. Chem. Lett*., 2013, **4**, 2073-2078.
9. C. Simpson, T. M. Clarke, R. W. MacQueen, Y. Y. Cheng, A. J. Trevitt, A. J. Mozer, P. Wagner, T. W. Schmidt and A. Nattestad, *Phys. Chem. Chem. Phys*., 2015, **17**, 24826-24830.
10. S. P. Hill, T. Banerjee, T. Dilbeck and K. Hanson*, J. Phys. Chem. Lett*., 2015, **6**, 4510-4517.
11. S. P. Hill, T. Dilbeck, E. Baduell and K. Hanson, *ACS Energy Lett*., 2016, **1**, 3-8.
12. T. Dilbeck, S. P. Hill and K. Hanson, *J. Mater. Chem. A.,* 2017, DOI: 10.1039/c7ta00317j.